Loading Rate Effects on Compressive Strength of Maha Sarakham Salt

Tanapol Sriapai, Pichit Samsri and Kittitep Fuenkajorn

Geomechanics Research Unit, Institute of Engineering, Suranaree University of Technology,

Muang District, Nakhon Ratchasima, Thailand 30000.

Phone (66-44) 224-758, Fax (66-44) 224-448

E-Mail: kittitep@sut.ac.th

Abstract

Uniaxial and triaxial compression tests are performed to assess the loading rate effect on the strength and deformability of the Maha Sarakham salt. The salt specimens with a nominal dimension of 5.4×5.4×5.4 cm^3 are compressed to failure using a polyaxial load frame. The lateral confining pressures are maintained constant at 0, 3, 7, 12, 20 and 28 MPa while the axial stresses are increased at constant rates of 0.001, 0.01, 0.1, 1.0 and 10 MPa/s until failure occurs. The salt elasticity and strength increase with the loading rates. The elastic modulus varies from 15 to 25 GPa, and the Poisson's ratio from 0.23 to 0.43. The elastic parameters tend to be independent of the confining pressures. The distortional strain energy at dilation and at failure from various loading rates varies linearly with the mean strain energy. The proposed empirical criteria are applied to determine the safe maximum withdrawal rate of a compressed-air energy storage cavern.

1. Introductions

The loading rate effect plays a significant role on the stability analysis and design of the pressure schemes for compressed-air, LPG, and natural gas storage caverns in salt [1]. Experimental and theoretical researches have long been performed, notably as part of nuclear waste disposal programs, to truly understand the time-dependent deformation (creep) of salt under the repository environments (e.g., elevated temperatures and pressures). Rare attempt, however, has been made to determine the rate-dependent strength of the salt, particularly under confined conditions. The strength criterion that can take the loading rate effects into consideration is also rare.

The objective of this research is to experimentally assess the influence of loading rate on the compressive strength and deformability of rock salt. Uniaxial and triaxial compression tests have been performed on Maha Sarakham salt using a polyaxial load frame with applied loading rates from 0.001 to 10 MPa/s, and confining pressures from 0 to 28 MPa. Multi-axial empirical criteria that can take loading rate effect into consideration are proposed to describe the dilation and failure of the salt. Supported by numerical simulations, these criteria are applied to calculate the factors of safety of salt around a compressed-air energy storage cavern subjected to various rates of pressure reduction during retrieval periods.

2. Salt Specimens

The tested specimens were prepared from 60 mm salt cores drilled from depths ranging between 140 m and 250 m by Pimai Salt Co. in the northeast of Thailand. The salt cores belong to the Middle Salt member of the Maha Sarakham formation. This salt member hosts several solution-mined caverns in the basin. The Maha Sarakham formation is also being considered as a host rock for compressed-air energy storage caverns by the Thai Department of Energy, and for chemical waste disposal by the Office of Atomic Energy for Peace. Warren [2] gives the origin and geological description

RECEIVED 21 April, 2011

ACCEPTED 4 October, 2011

of the Maha Sarakham salt. The tested salt is virtually pure halite, with a slight amount of clay inclusions (less than 1%). The drilled cores were dry-cut to obtain cubical shaped specimens with nominal dimensions of 5.4×5.4×5.4 cm^3. Over 40 specimens were prepared. No bedding plane was observed in the specimens. The average density is 2.19±0.09 g/cc.

3. Test Method

Polyaxial load frame [3] applies constant and uniform lateral stresses (confining pressures) to the salt specimen while the vertical stress is increased at a constant rate until failure occurs. The vertical stress is applied along the original axial direction of the salt core. The uniform lateral confining pressures ($\sigma_2 = \sigma_3$) on the salt specimens range from 0, 3, 7, 12, 20 to 28 MPa, and the constant vertical stress rates ($\partial\sigma_1/\partial t$) from 0.001, 0.01, 0.1, 1.0 to 10 MPa/s. After installing the cubical salt specimen into the load frame, dead weights are placed on the two lower bars to obtain the pre-defined magnitude of the uniform lateral stress (σ_3) on the specimen. Simultaneously the vertical stress is increased to the pre-defined σ_3 value. Neoprene sheets have been placed at the interface between loading platens and rock surfaces to minimize the friction. The test is started by increasing the vertical stress at the pre-defined rate using the electric pump. The specimen deformations are monitored in the three loading directions and are used to calculate the principal strains during loading. The readings are recorded every 10 kN of load increment until failure. The failure loads are recorded and the mode of failure is examined.

4. Test Results

Table 1 summarizes the results from all specimens, listing the major principal (vertical) stresses (σ_1) at failure for each lateral confining pressure (σ_3). The mean stresses (σ_m) and strains (ε_m) and the octahedral shear stresses ($\tau_{oct,f}$) and shear strains ($\gamma_{oct,f}$) at failure are also determined [4].

The rate-dependent shear strengths can be observed from the τ_{oct} - σ_m diagram, as shown in Figure 1. The test results show nonlinear relations between the octahedral shear stress and the mean stress at failure. The shear strength rapidly increases with mean stress and tends to approach an ultimate value for each loading rate ($\partial\sigma_1/\partial t$). Beyond the mean stress of 40 MPa and with the loading rate of 0.001 MPa/s the shear strength tends to be constant at about 21 MPa.

Table 2 lists the cohesion (c) and internal friction angle (ϕ) of the salt determined based on the Coulomb criterion [4]. The cohesion ranges from 4.0 to 5.3 MPa, and the friction angle from 40.4 to 46.6 degrees. They are calculated at the confining pressure of 7 MPa for all loading rates. Both increase with the loading rate, suggesting that the salt is stronger under higher loading rates.

5. Elastic Properties of Maha Sarakham Salt

The elastic modulus and Poisson's ratio for each specimen are determined from the tangent of the stress-strain curves at 50% failure stress (Table 3). Based on this calculation the elastic modulus of the salt appears to increase with loading rate. It ranges from 15 to 25 GPa. The Poisson's ratio of the salt ranges from 0.23 to 0.43, and tends to be and tends to be independent of the loading rate. The effect of the confining pressure on the salt elasticity and Poisson's ratio can not be clearly observed from the test results. This is probably due to the intrinsic variability among the specimens.

6. Octahedral Shear Stress and Shear Strain Relation

This section proposes shear strength and dilation criteria that take the corresponding shear strains into account. From the test results the octahedral shear stress can be calculated as a function of shear strain at failure and at dilation for various mean stress magnitudes, as shown in Figure 2. The italic

Table 1 Salt strengths and elastic properties under various loading rates and confining pressures.

Specimen No.	$\partial\sigma_1/\partial t$ (MPa/s)	σ_3 (MPa)	σ_1 (MPa)	σ_m (MPa)	ε_m (10^{-3})	$\tau_{oct,f}$ (MPa)	$\gamma_{oct,f}$ (10^{-3})	E (GPa)	ν
31	10	0	25.1	8.4	-	11.8	-	-	-
7	1		22.6	7.5	-	10.7	-	21.4	-
6	0.5		20.4	6.8	-	9.6	-	19.9	-
9	0.1		19.2	6.4	-	9.1	-	19.5	-
11	0.05		19.1	6.4	-	9.0	-	19.3	-
10	0.01		17.8	5.9	-	8.4	-	18.2	-
8	0.005		17.8	5.9	-	8.4	-	17.8	-
12	0.001		16.5	5.5	-	7.8	-	15.7	-
35	10	3	49.5	18.5	-	21.9	-	-	-
33	1		45.3	17.1	-3.2	19.9	25.8	22.5	0.25
32	0.1		42.5	16.2	-1.0	18.6	27.9	21.8	0.26
38	0.01		41.2	15.7	-4.8	18.0	33.3	19.6	0.24
16	0.001		37.5	14.5	-3.1	16.3	37.9	15.6	0.31
34	10	7	69.0	27.7	-	29.2	-	-	-
41	1		64.8	26.3	-0.6	27.2	30.1	21.7	0.29
29	0.1		60.3	24.8	-3.2	25.1	33.1	17.6	0.32
27	0.01		57.4	23.8	-6.3	23.8	35.6	17.9	0.27
20	0.001		48.1	20.7	-6.0	19.4	37.1	16.9	0.32
43	10	12	88.9	37.6	-0.8	36.3	23.3	22.6	0.24
39	1		81.8	35.3	-1.7	32.9	27.3	22.7	0.33
17	0.1		72.8	32.3	-4.1	28.7	35.1	19.8	0.38
26	0.01		66.0	30.0	-6.3	25.5	36.1	19.0	0.35
15	0.001		54.8	26.3	-6.0	20.2	36.8	17.8	0.38
40	10	20	106.4	48.8	-0.3	40.7	23.8	22.0	0.23
18	1		96.2	45.4	-0.5	35.9	27.2	21.9	0.39
42	0.1		87.5	42.5	-1.4	31.8	30.7	19.1	0.43
30	0.01		78.3	39.4	-0.8	27.5	36.6	19.9	0.40
23	0.001		64.8	34.9	-0.4	21.1	42.1	17.5	0.42
22	10	28	119.7	58.6	-0.2	43.2	25.1	25.2	0.24
44	1		109.0	55.0	-0.4	38.2	28.7	23.0	0.36
37	0.1		99.2	51.7	-0.5	33.6	32.7	19.8	0.42
45	0.01		87.4	47.8	-0.5	28.0	39.0	17.2	0.43
46	0.001		73.6	43.2	-2.9	21.5	45.4	16.7	0.43

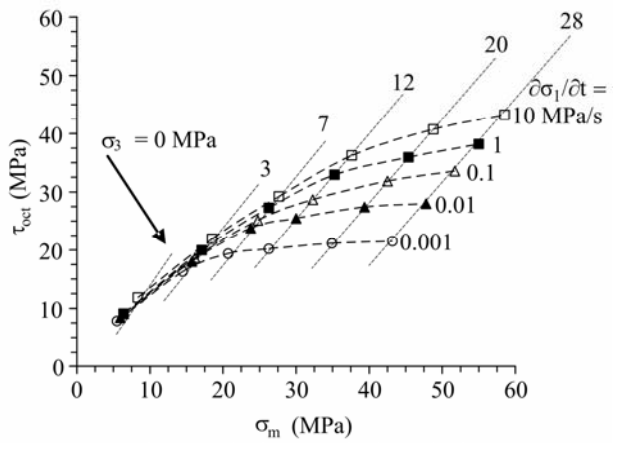

Figure 1 Octahedral shear stress (τ_{oct}) at failure as a function of mean stress (σ_m) for various confining pressures (σ_3) and loading rates ($\partial\sigma_1/\partial t$).

Table 2 Cohesion and friction angle of salt calculated at σ_3=7 MPa.

$\partial\sigma_1/\partial t$ (MPa/s)	ϕ (Degrees)	c (MPa)
10	46.6	5.3
1	45.7	4.9
0.1	45.3	4.3
0.01	44.7	4.1
0.001	40.4	4.0

Table 3 Material properties and loading parameters used in FLAC simulations.

Parameters	Values
E_1 (GPa)	1.90
E_2 (GPa)	5.79
η_1 (GPa.Day)	0.34
η_2 (GPa.Day)	0.05
γ (g/cc)	2.20
In-situ stress at casing shoe, σ_{cs} (MPa)	10.8
P_i at 90% σ_{cs} (MPa)	9.7
P_i at 20% σ_{cs} (MPa)	2.2
P_i at 10% σ_{cs} (MPa)	1.1

$\tau_{oct,f} = A\,\gamma_{oct,f}^{-\alpha}$

σ_m (MPa)	A (MPa)	α
50	422.9	0.71
40	391.9	0.72
30	380.6	0.74
20	327.8	0.77

$A = 150\sigma_m^{0.26}$

$\alpha = \sigma_m^{-0.09}$

$\tau_{oct,d} = A'\,\gamma_{oct,d}^{-\alpha'}$

σ_m (MPa)	A′ (MPa)	α'
50	113.7	0.46
40	111.4	0.51
30	104.3	0.56
20	98.8	0.65

$A' = 60.9\sigma_m^{0.16}$

$\alpha' = 2\sigma_m^{-0.37}$

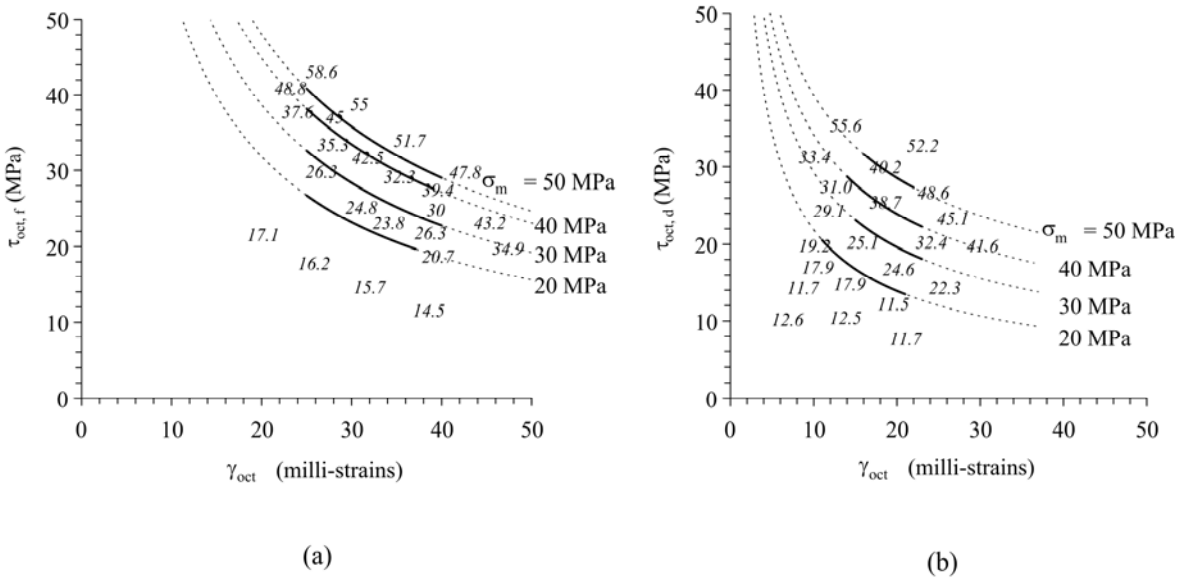

(a) (b)

Figure 2 Octahedral shear stress at failure (a) and at dilation (b) as a function of octahedral shear strain for various mean stresses.

numbers in Figure 2 represent the magnitudes of σ_m where their locations indicate the corresponding magnitudes of the octahedral shear stress and strain at failure ($\tau_{oct,f}$) and at dilation ($\tau_{oct,d}$). Sets of empirical (power) equations can be used to determine the variation of the octahedral shear stress with the octahedral shear strain at failure and at dilation for the selected σ_m magnitudes of 20, 30 40 and 50 MPa. They can be written as:

$$\tau_{oct,f} = A \cdot (\gamma_{oct,f})^{-\alpha} \quad (1)$$

$$\tau_{oct,d} = A' \cdot (\gamma_{oct,d})^{-\alpha'} \quad (2)$$

where A, A′, α and α' are shear strain constants and shear strain exponents for the salt at failure and at dilation, respectively. For the Maha Sarakham salt they can be empirically defined as a function of σ_m, as follows:

$$A = 150\sigma_m^{0.26} \text{ MPa; and } \alpha = \sigma_m^{-0.09} \quad (3)$$

$$A' = 60.9\sigma_m^{0.16} \text{ MPa; and } \alpha' = 2\sigma_m^{-0.37} \quad (4)$$

By substituting Eqs. (3) and (4) into Eqs. (1) and (2), the failure and dilation criteria of the salt can be presented in forms of the octahedral shear stress and strain:

$$\tau_{oct,f} = 150\sigma_m^{0.26} \cdot (\gamma_{oct.f})^{-\sigma_m^{-0.09}} \quad (5)$$

$$\tau_{oct,d} = 60.9\sigma_m^{0.16} \cdot (\gamma_{oct.d})^{-2\sigma_m^{-0.37}} \quad (6)$$

The numerical values of these constants and their corresponding σ_m magnitudes are given in Figure 2. Eqs. (5)

and (6) consider both the applied shear stresses and the induced shear strains, and hence implicitly incorporate the effects of loading rate on the salt strength and dilation.

7. Strain Energy Density Criteria

The strain energy density principle is applied here to describe the salt strength and deformability under different loading rates. A similar approach has been used by Fuenkajorn and Kenkhunthod [3] to derive a loading rate-dependent strength criterion for sandstones. The distortional strain energy at failure (W_d) and at dilation ($W_{d,d}$) can be calculated from the octahedral shear stresses and strains for each salt specimen using the following relations [4]:

$$W_d = (3/2) \cdot \tau_{oct,f} \cdot \gamma_{oct,f} \quad (7)$$

$$W_{d,d} = (3/2) \cdot \tau_{oct,d} \cdot \gamma_{oct,d} \quad (8)$$

It is assumed that under a given mean stress the distortional strain energy required to dilate and to fail the salt specimens are constant.

Regression on the test results indicates that the distortional strain energy linearly increases with the mean stress:

$$W_d = \kappa \cdot \sigma_m + \lambda \quad (9)$$

$$W_{d,d} = \kappa' \cdot \sigma_{m,d} + \lambda' \quad (10)$$

where κ, κ', λ and λ' are empirical constants. For the Maha Sarakham salt they are defined as: κ = 27.9; λ = 932 MPa; κ' = 29.1; and λ' = 171 MPa. Eqs. (9) and (10) can be used to predict the salt strength and dilation in terms of the maximum distortional strain energy that a salt can absorb before failure or dilation occurs. The distortional strain energy at dilation ($W_{d,d}$) can also be derived as a function of the mean strain energy density at dilation ($W_{m,d}$). Figure 3 shows a linear trend of the test data in the $W_{d,d}$ - $W_{m,d}$ diagram which can be represented by:

$$W_{d,d} = \chi \cdot W_{m,d} + \xi \quad (11)$$

For the Maha Sarakham salt, χ = 4.0 and ξ = 91.9 MPa. The $W_{d,d}$ - $W_{m,d}$ criterion (eq. 11) explicitly considers both octahedral shear and mean stresses and strains. Hence it can describe the salt dilation more comprehensively than the criteria developed earlier.

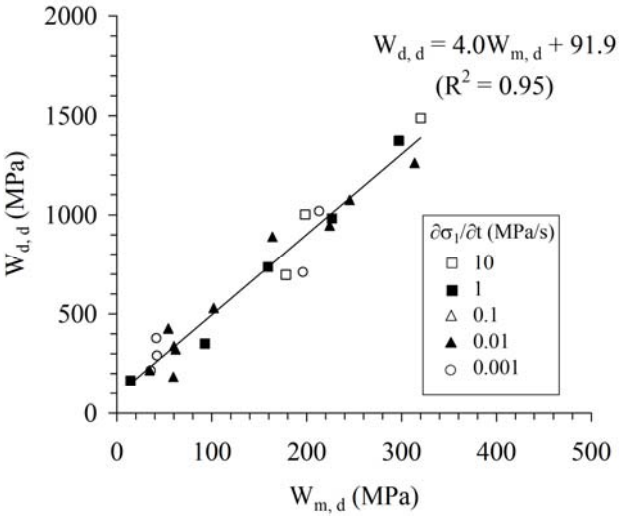

Figure 3 Distortional strain energy at dilation ($W_{d,d}$) as a function mean strain energy at dilation ($W_{m,d}$).

8. Withdrawal Rate of Compressed-Air Energy Storage (CASE) Cavern

This section describes an application of the rate-dependent dilation criteria derived earlier. They are used to determine the safe maximum withdrawal rate of a CAES cavern in the Maha Sarakham salt formation. The finite difference program – FLAC [5] is used in the simulations of the single isolated cavern in axial symmetry. The principal stresses and strains induced in the surrounding salt under various air withdrawal rates are calculated and compared against the dilation criteria developed above. Figure 4 shows the mesh

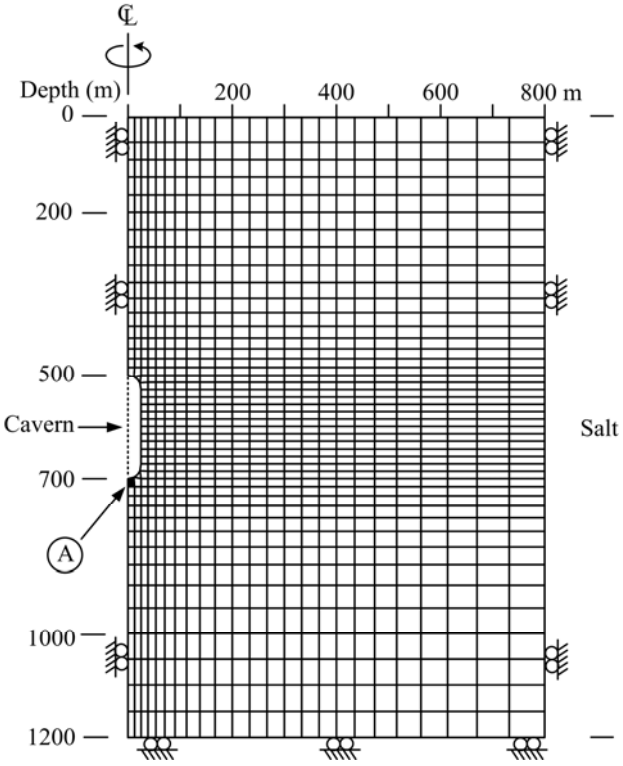

Figure 4 Finite difference mesh developed for FLAC simulation of CAES cavern.

model representing the cavern from the ground surface to the depth of 1200 m. The depth at the top of the cavern is taken as 500 m. The cavern diameter is 50 m, and its height is 200 m. It has a half-spherical roof and bottom. The cavern configurations, depth and site geology used here represent a preliminary design of the CAES cavern in the Khorat basin in the northeast of Thailand.

The in-situ stress is assumed to be hydrostatic. Before cavern development the salt stress at the casing shoe depth (σ_{cs}) is calculated as 10.8 MPa. The maximum cavern pressure is defined as 9.7 MPa (or $0.9\sigma_{cs}$). Two cases with different minimum pressures are studied: 1.1 MPa and 2.2 MPa ($0.1\sigma_{cs}$ and $0.2\sigma_{cs}$). Each case is simulated for four different rates of cavern pressure withdrawal: 17.3, 8.6, 0.6 and 0.3 MPa/day (equivalent to pressure schemes of 1 cycle/day, 15 cycles/month, 1 cycle/month and 6 cycles/year, respectively). The Maha Sarakham salt is assumed to behave as a Burgers material. The Burgers constitutive equation is a built-in program in FLAC. It can be written as [4, 6]:

$$\sigma + \left\{\left(\frac{\eta_1}{E_1}\right)+\left(\frac{\eta_2}{E_2}\right)+\left(\frac{\eta_1}{E_2}\right)\right\}\cdot\left(\frac{\partial\sigma}{\partial t}\right)+ \left\{\frac{\eta_1\eta_2}{E_1E_2}\cdot\left(\frac{\partial^2\sigma}{\partial t^2}\right)\right\} = \eta_1\cdot\left(\frac{\partial\varepsilon}{\partial t}\right)+\left\{\frac{\eta_1\eta_2}{E_2}\cdot\left(\frac{\partial^2\varepsilon}{\partial t^2}\right)\right\} \quad (12)$$

The spring constants (E_1 and E_2) and viscosity coefficients (η_1 and η_2) of the Burgers model for the Maha Sarakham salt are given in Table 3. They are obtained from creep testing of the same salt by Samsri [7].

Tables 4 and 5 summarize the simulation results for the two cases in terms of the octahedral shear stresses and strains, and distortional and mean strain energy at the bottom of the cavern (point A – Figure 4). They are calculated at 24 hours after starting withdrawal. The stability of the cavern bottom is of interest in this analysis because during withdrawal it will be subject to the largest difference between the internal air pressure and the salt in-situ stress. The octahedral shear stresses and strains for the minimum pressure of 1.1 MPa are slightly greater than those for the 2.2 MPa. For a conservative design the surrounding salt is not allowed to dilate during the withdrawal period. This is to ensure the long-term stability of the storage cavern under the cyclic loading. As a result the two dilation criteria are used here to calculate the factor of safety (FS) of the salt at the bottom of the cavern. These include $\tau_{oct,d} - \gamma_{oct,d}$ criterion (eq. 6) and $W_{d,d}$ - $W_{m,d}$ criterion (eq. 11). The FS calculation methods and results for all pressure schemes are shown in Tables 4 and 5. The two criteria give different FS values. Bath criteria however agree that when the minimum pressure of 1.1 MPa ($0.1\sigma_{cs}$) is applied, the salt will dilate under the pressure withdrawal rate of 15.1 MPa/day (1 cycle/day). The $\tau_{oct,d}$ - $\gamma_{oct,d}$ criterion tends to give the largest FS values for all cases. This criterion

Table 4 Factor of safety at cavern bottom based on $\tau_{oct,d}$–$\gamma_{oct,d}$ criterion.

Pressure Scheme	$\tau_{oct,d} = A'\gamma_{oct,d}^{-\alpha}$				Factor of Safety (FS = $\tau_{oct,d}$ / τ_{oct})	
	P_i = 90% → 20%		P_i =90% → 10%			
	A'	α'	A'	α'	P_i = 90% → 20%	P_i = 90% → 10%
1 cycle/day	96.4	0.69	96.7	0.68	1.10	0.98
15cycles/month	96.2	0.69	96.4	0.69	1.34	1.21
1 cycle/month	94.9	0.72	94.9	0.72	3.69	3.63
6 cycles/yr	94.8	0.72	94.8	0.72	3.90	3.87

Table 5 Factor of safety at cavern bottom based on $W_{d,d}$ - $W_{m,d}$ criterion.

Pressure Scheme	$W_{d,d} = 4W_{m,d} + 91.9$ (MPa)				Factor of Safety (FS = $\tau_{oct,d}$ / τ_{oct})	
	P_i = 90% → 20%		P_i =90% → 10%			
	A'	α'	A'	α'	P_i = 90% → 20%	P_i = 90% → 10%
1 cycle/day	17.3	161.1	20.3	172.9	0.35	0.33
15cycles/month	16.7	158.9	17.6	162.2	0.44	0.40
1 cycle/month	11.7	138.8	11.8	139.0	1.32	1.30
6 cycles/yr	11.6	138.1	11.6	138.2	1.40	1.39

does not consider the mean stresses and strains induced around the cavern. The simulation results indicate that the safe withdrawal rate can be increased by raising the minimum storage pressure. As shown in Tables 4, for all criteria the factors of safety calculated for the 20% minimum pressure are about 5-10% greater than those for the 10%. The $W_{d,d}$ - $W_{m,d}$ criterion (Table 5) gives the most conservative results. It shows the FS values lower than 1.0 for the withdrawal rates of 15.1 and 7.6 MPa/day (1 cycle/day and 15 cycles/month). This criterion is perhaps the most appropriate for use in the design of the withdrawal rate because it incorporates both shear and mean stresses and strains.

9. Discussions and Conclusions

The results indicate that the elastic modulus and failure stresses increase with the loading rates. These agree well with the experimental results on rock salt performed by Mikhalyuk et al. [8] and Liang et al. [9]. The salt elastic modulus measured at 50% failure stress varies from 15 to 25 GPa, and the Poisson's ratio from 0.23 to 0.43. Both tend to be independent of the confining pressures. The rate effects on the Poisson's ratio can not be clearly seen here, probably due to the intrinsic variability of the salt. Under the range of the tested parameters the salt shows highly non-linear behavior which can be clearly seen in the τ_{oct} - σ_m diagram (Figure 1). Both salt strength and stiffness increase with the loading rate, as experimentally evidenced by the increase of the internal friction angle, cohesion, failure stress, and elastic modulus. Several forms of the strength and dilation criteria have been derived. The $W_{d,d}$ - $W_{m,d}$ criterion (eq. 11) is the most comprehensive formulation, and perhaps is the most reliable. It implicitly incorporates the rate effect, and requires complete stress-strain relations that must be obtained from compression testing under various loading rates. The shear strains induced at dilation and failure are added into the formulation of the $\tau_{oct,f}$ - $\gamma_{oct,f}$ and $\tau_{oct,d}$ - $\gamma_{oct,d}$ criteria (eqs. 1 and 2) to implicitly consider the rate effect. This should improve their reliability for describing the salt strength and dilation. The CAES cavern simulations is an example for the application of the rate dependent dilation criteria. This is primarily to demonstrate that the criteria derived in this paper can be used to assist in the design and stability analysis for practical problems. The applicability of the proposed criteria and the FS calculation results are encouraging.

10. Acknowledgements

The work was funded by Suranaree University of Technology. Permission to publish this paper is gratefully acknowledged. We would like to thank Pimai Salt Co. for donating salt cores used in this study.

References

[1] Jeremic KL (1994) Rock Mechanics in Salt Mining. Rotterdam: A.A. Balkema.

[2] Warren J (1999) Evaporites: Their Evolution and Economics. Oxford: Blackwell Science.

[3] Fuenkajorn K, Kenkhunthod N (2010) Influence of loading rate on deformability and compressive strength of three Thai sandstones. Geotechnical and Geological Engineering 28: 707-715.

[4] Jaeger JC, Cook, NGW, Zimmerman RW (2007) Fundamentals of Rock Mechanics. Fourth Edition, Oxford: Blackwell Publishing.

[5] Itasca (1992) User Manual for FLAC-Fast Langrangian Analysis of Continua, Version 4.0. Itasca Consulting Group Inc., Minnesota: Minneapolis.

[6] Findley WN, Lai SJ, Onaran K (1989) Creep and Relaxation of Nonlinear Viscoelastic Materials: with an introduction to linear viscoelasticity. New York: Courier Dover.

[7] Samsri P (2010) Determination of creep properties of rock salt using modified point load testing. M.S. Thesis. Nakhon Ratchasima: Suranaree University of Technology.

[8] Mikhalyuk AV, Zakharov VV, Parshukov PA (1998) Rock salt under nonequilibrium dynamic loads. Journal of Mining Science 34(1): 1-9.

[9] Liang WG, Zhao, YS, Xu SG, Dusseault MB (2010) Effect of strain rate on the mechanical properties of salt rock. Int. J. Rock Mech. Min. Sci. 48(1): 161-167.